Theor Chim Acta (1987) 71: 479-487

Theoretica Chimica Acta

Theory of angle-resolved photoemission for in general disordered complex lattices: applications to the off-normal emission from TiN_x (100)

Dedicated to Professor H. Nowotny on the occasion of his 75th birthday

J. Redinger[1]*, P. Weinberger[1], and A. Neckel[2]

[1] Institut für Technische Elektrochemie, Technische Universität Wien, A-1090 Wien
[2] Institut für Physikalische Chemie, Universität Wien, Währingerstr. 42, A-1090 Wien, Austria

(Received January 5, revised March 5/Accepted March 10, 1987)

The theory of angle resolved photoemission for in general disordered complex lattices of semi-infinite solid systems is presented. An application of this theory to the He-I off-normal photoemission spectra from $TiN_{0.83}$ (100) reveal the same kind of vacancy-like related peaks observed for powder samples in angle integrated spectra in the UPS and XPS regime.

Key words: Disordered complex lattices — Photoemission

1. Introduction

Photoemission is the most successful single experimental technique to map the electronic structure of surface near regions in solids. Because exactly these regions are of crucial importance for many material properties, it is absolutely necessary not only to describe the electronic structure of solids with surface properly, but also to calculate directly physical observables such as for example photoemission intensities.

In the present paper the theory of angle resolved photoemission (ARPES) is formulated for in general complex, disordered lattices of semi-infinite solid systems. The present theory is applicable to calculations of the photocurrent for

* *Present address*: Department of Physics and Astronomy, Northwestern University, Evanston, Il, USA

ordered or disordered, stoichiometric or non-stoichiometric systems. The theoretical description is based on Pendry's [1] inverse LEED formalism and its generalization to disordered simple lattices by Durham [2]. The actual computer codes made partially use of Larsson's [3] NEWPOOL-code for ARUPS of ordered complex lattices.

The paper is organized as follows: Sect. 2 presents the theoretical approach involved, in Sect. 3 computational details are discussed briefly. Section 4 gives results for a very typical problem in dealing with "real" systems, namely the angle resolved photoemission from a single crystal non-stoichiometric refractory phase surface. For the example chosen, $TiN_{0.83}$ (100), comparison is made also to experimental and theoretical angle integrated photoemission studies in the UPS and XPS regime.

2. Theoretical approach

For complex lattices the unit cell Ω_i is a sum of subcells Ω_{is} corresponding to the sublattices s

$$\Omega_i = \sum_s \Omega_{is}. \tag{1}$$

The non-cell diagonal scattering path operators $\mathbb{T}^{ij}$ are supermatrices (Klima et al. [8]), where each element is an angular momentum representative of a non-site diagonal scattering path operator corresponding to the one particle Green's functions in the following way, $\boldsymbol{r} = \boldsymbol{r}_{is} + \boldsymbol{R}_{is}$, $\boldsymbol{r}' = \boldsymbol{r}'_{js} + \boldsymbol{R}_{js}$, $L = (lm)$,

$$G(\boldsymbol{r}, \boldsymbol{r}', E) = \sum_{L,L'} \{Z_L^{is}(\boldsymbol{r}_{is}, E)\tau_{ss',LL'}^{ij}(E)Z_{L'}^{js'}(\boldsymbol{r}'_{js'}, E) - \delta_{LL'}\delta_{ij}\delta_{ss'}Z_L^{is}(\boldsymbol{r}_{is}, E)J_{L'}^{js}(\boldsymbol{r}_{js'}, E)\} \tag{2}$$

whereby $Z_L^{is}(\boldsymbol{r}_{is}, E)$ and $J_L^{is}(\boldsymbol{r}_{is}, E)$ are the scattering solutions discussed in the review article by Faulkner [4]. $Z_L^{is}(\boldsymbol{r}_{is}, E)$ is regular at the origin, whereas $J_L^{is}(\boldsymbol{r}_{is}, E)$ is in general not regular at the origin. For translationally invariant materials (pure phases, effective lattices), the cell-diagonal operators can be evaluated easily by means of the following BZ integral

$$\mathbb{T}^{ii} = \frac{1}{\Omega_{BZ}} \int [\mathbb{t}^{-1} - \mathbb{g}(\boldsymbol{k})]^{-1} \, \mathrm{d}\boldsymbol{k} \tag{3}$$

where the $\mathbb{g}(\boldsymbol{k})$ are nothing but the usual KKR-type structure constants for complex lattices (Ham and Segall [5]). As will be shown later, the cell-diagonal scattering path operators are central quantities for a description of photoemission from disordered complex lattices.

If photons of energy ω and a given polarisation are incident at a given angle to the crystal surface normal (taken to be the z-direction), the current of photoelectrons with energy $E + \omega$ and momentum $\boldsymbol{k}_\parallel$ parallel to the surface passing through

a plane $z = z_0$ (detector) is given in a one-electron approximation as (Hopkinson et al [6], Durham [2])

$$I_{k_\parallel} = \pi^{-1} \operatorname{Im} \int\int d\boldsymbol{r}\, d\boldsymbol{r}'\, \psi_2(\boldsymbol{r}, E+\omega)\, \Delta(\boldsymbol{r}) G(\boldsymbol{r}, \boldsymbol{r}', E)\, \Delta^*(\boldsymbol{r}') \psi_2^*(\boldsymbol{r}', E+\omega) \tag{4}$$

where $G(\boldsymbol{r}, \boldsymbol{r}', E)$ is the one-electron Green's function at energy E (2), $\psi_2(\boldsymbol{r}, E+\omega)$, the LEED state, is

$$\psi_2(\boldsymbol{r}, E+\omega) = \int d\boldsymbol{r}'\, \delta(z - z_0)\, e^{-i\boldsymbol{k}_\parallel \cdot \boldsymbol{r}_\parallel} G(\boldsymbol{r}, \boldsymbol{r}', E) \tag{5}$$

and the electron-photon interaction $\Delta(\boldsymbol{r})$ is

$$\Delta(\boldsymbol{r}) = \frac{2i\sqrt{2}}{\omega c} \boldsymbol{A} \cdot \nabla V(\boldsymbol{r}). \tag{6}$$

In (6) $\boldsymbol{A}$ is the vector potential, $V(\boldsymbol{r})$ the effective potential, corresponding to the Kohn-Sham equations of the system under consideration and c is the speed of light.

In the following we want to restrict ourselves to complex lattices with two sublattices only. Extensions to more than 2 sublattices are straightforward using a supermatrix notation.

For $\boldsymbol{r} = \boldsymbol{r}_{is} + \boldsymbol{R}_{is}$ lying inside the i-th sphere of the sublattice s, the LEED function can be written in terms of the usual multiple scattering expansions (see e.g. Durham [2])

$$\psi_2(\boldsymbol{r}_{is}, E+\omega) = \sum_j \sum_{s_1, s_2} \sum_{L_1, L_2, L_3} \{ f^0_{s_1, L_1}(E+\omega) g^{0j}_{s_1 s_2, L_1 L_2}(E+\omega) \tau^{ji}_{s_2 s_1 L_2 L_3} \times (E+\omega) Z^{is}_{L_3}(\boldsymbol{r}_{is}, E+\omega) \} \tag{7}$$

where $g^{ij}_{SS', LL'}(E+\omega)$ is a free-electron real space propagator and $f^0_{S,L}(E+\omega)$ is given by the following integral

$$f^0_{S,L}(E+\omega) = \int d\Omega_s\, \delta(z_s - z^0_s)\, e^{-i\boldsymbol{k}_\parallel \cdot \boldsymbol{r}_{0s,\parallel}} j_l(\sqrt{E+\omega}\, |\boldsymbol{r}_{0s}|)\, Y_L(\hat{\boldsymbol{r}}_{0s}). \tag{8}$$

From (4) one can see that the photocurrent $I_{k_\parallel}$ can be written as follows

$$I_{k_\parallel} = -\pi^{-1} \operatorname{Im} \sum_{i,j} \operatorname{tr} \{ (\mathbb{M}^i)^+ \mathbb{t}^{ij} \mathbb{M}^j + \delta_{ij} \mathbb{I}^i_a \} \tag{9}$$

where $\mathbb{M}^i$ is a supermatrix of the form

$$\mathbb{M}^i = \begin{pmatrix} \boldsymbol{M}^{is} & \boldsymbol{O} \\ \boldsymbol{O} & \boldsymbol{M}^{is'} \end{pmatrix} \tag{10}$$

each block being a diagonal matrix of elements M^{is}_L

$$M^{is}_L = \int d\Omega_{is}\, \psi_2(\boldsymbol{r}_{is}, E+\omega) \Delta_{is}(\boldsymbol{r}_{is}) Z^{is}_L(\boldsymbol{r}_{is}, E). \tag{11}$$

According to the muffin-tin approximation applied, the isth contribution to the electron-photon interaction is

$$\Delta(\boldsymbol{r}) = \sum_{i,s} \Delta_{is}(\boldsymbol{r}_{is}) = \frac{2i\sqrt{2}}{\omega c} \sum_{i,s} \boldsymbol{A} \cdot \nabla V_{is}(\boldsymbol{r}_{is}) \tag{12}$$

The supermatrix $\mathbb{I}_a^i$ in (9) contains all the intra-atomic contributions to the photocurrent (see also Durham [2])

$$\mathbb{I}_a^i = \begin{pmatrix} \boldsymbol{I}_{is}^a & \boldsymbol{O} \\ \boldsymbol{O} & \boldsymbol{I}_{is'}^a \end{pmatrix}. \tag{13}$$

In (13) the blocks $\boldsymbol{I}_{is}^a$ are diagonal matrices of elements $I_{is,L}^a$

$$I_{is,L}^a = \pi^{-1} \operatorname{Im} \iint d\boldsymbol{r}_{is}\, d\boldsymbol{r}'_{is} \{\psi_2(\boldsymbol{r}_{is}, E+\omega)\Delta_{is}(\boldsymbol{r}_{is}) \times Z_L^{is}(\boldsymbol{r}_{is}, E) J_L^{is}(\boldsymbol{r}'_{is}, E)\Delta_{is}^*(\boldsymbol{r}'_{is})\psi_2^*(\boldsymbol{r}'_{is}, E+\omega)\}. \tag{14}$$

The trace in (9) implies also a sum over sublattices

$$\operatorname{tr}\{(\mathbb{M}^i)^+ \mathbb{T}^{ij} \mathbb{M}^j\} = \sum_s \operatorname{tr}\{(\boldsymbol{M}^{is})^+ \boldsymbol{\tau}_{ss}^{is} \boldsymbol{M}^{js}\}. \tag{15}$$

Applying for disordered systems the same type of averaging as was suggested by Durham [2] for simple lattices, the restricted average for the triple product of matrices (Green's functions) in (15) is given by

$$\langle (\boldsymbol{M}^{is})^+ \boldsymbol{\tau}_{ss}^{ij} \boldsymbol{M}^{js} \rangle_{is\alpha, js\beta} = (\boldsymbol{M}^{is,\alpha})^+ \langle \boldsymbol{\tau}_{ss}^{ij} \rangle_{is\alpha, js\beta} \boldsymbol{M}^{js,\beta} \tag{16}$$

whereby the suffices $is\alpha$ and $js\beta$ mean that the sites is and js are occupied by species α and β, respectively. The restricted averages of the sublattice diagonal scattering path operators $\langle \boldsymbol{\tau}_{ss}^{ij} \rangle$ are given by Schadler et al. [7]

$$\langle \boldsymbol{\tau}_{ss}^{ij} \rangle_{is\alpha, js\beta} = [\mathbb{D}^{\alpha,ii} \mathbb{T}_c^{ij} \mathbb{D}^{\beta,jj}]_{ss} \tag{17}$$

$$\langle \boldsymbol{\tau}_{ss}^{ii} \rangle_{is\alpha} = [\mathbb{D}^{\alpha,ii}\ {}_c^{ii}]_{ss} \tag{18}$$

whereby ${}_c^{ii}$ is the cell-diagonal effective scattering path operator built up by blocks $\tau_{c,ss'}^{ii}$. The supermatrix $\mathbb{D}^{\alpha,ii}$, sometimes also called "impurity matrix", is given by

$$\mathbb{D}^{\alpha,ii} = [\mathbb{1} + \mathbb{\Delta}^{\alpha,ii} \mathbb{T}_c^{ii}]^{-1} = \begin{pmatrix} \boldsymbol{D}_{ss}^{\alpha,ii} & \boldsymbol{D}_{ss'}^{\alpha,ii} \\ \boldsymbol{D}_{s's}^{\alpha,ii} & \boldsymbol{D}_{s's'}^{\alpha,ii} \end{pmatrix} \tag{19}$$

$$\mathbb{\Delta}^{\alpha,ii} = \begin{pmatrix} \boldsymbol{\Delta}_s^{\alpha,ii} & \boldsymbol{O} \\ \mathrm{O} & \boldsymbol{\Delta}_{s's'}^{\alpha,ii} \end{pmatrix} \tag{20}$$

$$\boldsymbol{\Delta}_{ss}^{\alpha,ii} = (\boldsymbol{t}_{ss}^{\alpha,ii})^{-1} - (\boldsymbol{t}_{ss}^{c,ii})^{-1}. \tag{21}$$

In (21) $\boldsymbol{t}_{ss}^{\alpha,ii}$ is the single site t-matrix of constituent α on the sth sublattice in the ith cell and $\boldsymbol{t}_{ss}^{c,ii}$ is the corresponding effective scattering t-matrix.

Restricting the alloying process to one sublattice only (pseudobinary alloys) and denoting by $s=1$ the alloyed sublattice and by $s=2$ the pure sublattice, $\boldsymbol{\Delta}_{ss}^{\alpha,ii}$ in (21) is reduced to

$$\boldsymbol{\Delta}_{ss}^{\alpha,ii} = \boldsymbol{\Delta}_{ss}^{\alpha,ii} \delta_{1s}. \tag{22}$$

For pseudobinary alloys with components A and B on sublattice $s=1$ and component X on sublattice $s=2$ (pure lattice), the average over the restricted averages in [17, 18) is given by Schadler et al. [7]. The triple product of matrices in (16) is therefore given by the following expression

$$\langle (\boldsymbol{M}^{is})^{+} \boldsymbol{\tau}_{ss}^{ij} \boldsymbol{M}^{js} \rangle = \begin{cases} \sum\limits_{\alpha,\beta=A,B} c_\alpha c_\beta (\boldsymbol{M}_{11}^{i\alpha})^{+} \boldsymbol{D}_{11}^{\alpha,ii} \boldsymbol{\tau}_{c,11}^{ij} \boldsymbol{D}_{11}^{\beta,jj} \boldsymbol{M}_{11}^{j\beta}; & s=1 \\ (\boldsymbol{M}_{22}^{iX})^{+} \boldsymbol{\tau}_{c,22}^{ij} \boldsymbol{M}_{22}^{jX}; & s=2 \end{cases} \tag{23}$$

$$\langle (\boldsymbol{M}^{is})^{+} \boldsymbol{\tau}_{ss}^{ii} \boldsymbol{M}^{is} \rangle = \begin{cases} \sum\limits_{\alpha=A,B} c_\alpha (\boldsymbol{M}_{11}^{i\alpha})^{+} \boldsymbol{D}_{11}^{\alpha,ii} \boldsymbol{\tau}_{c,11}^{ii} \boldsymbol{M}_{11}^{i\alpha}; & s=1 \\ (\boldsymbol{M}_{22}^{iX})^{+} \boldsymbol{\tau}_{c,22}^{ii} \boldsymbol{M}_{22}^{iX}; & s=2 \end{cases} \tag{24}$$

Putting now all terms together, the photocurrent for a pseudobinary alloy is given by

$$\begin{aligned} I_{k_\parallel} = -\pi^{-1} \operatorname{Im} \Bigg[& \sum_i \operatorname{tr} \left\{ (\boldsymbol{M}_{22}^{iX})^{+} \boldsymbol{\tau}_{c,22}^{ii} \boldsymbol{M}_{22}^{iX} + \sum_{\alpha=A,B} c_\alpha (\boldsymbol{M}_{11}^{i\alpha})^{+} \boldsymbol{D}_{11}^{\alpha,ii} \boldsymbol{\tau}_{c,11}^{ii} \boldsymbol{M}_{11}^{i\alpha} \right\} \\ & + \sum_{\substack{i,j \\ i \neq j}} \operatorname{tr} \left\{ (\boldsymbol{M}_{22}^{iX})^{+} \boldsymbol{\tau}_{c,22}^{ij} \boldsymbol{M}_{22}^{jX} + \sum_{\alpha,\beta=A,B} c_\alpha c_\beta (\boldsymbol{M}_{11}^{i\alpha})^{+} \boldsymbol{D}_{11}^{\alpha,ii} \boldsymbol{\tau}_{c,11}^{ij} \boldsymbol{D}_{11}^{\beta,jj} \boldsymbol{M}_{11}^{j\beta} \right\} \\ & + \sum_i \operatorname{tr} \{ \langle \boldsymbol{I}_{i,1}^{a} \rangle + \boldsymbol{I}_{i2,X}^{a} \} \Bigg] \end{aligned} \tag{25}$$

$$\langle \boldsymbol{I}_{i,1}^{a} \rangle = c_A \boldsymbol{I}_{i1,A}^{a} + c_B \boldsymbol{I}_{i1,B}^{a}. \tag{26}$$

It should be noted that the present theoretical result is not necessarily restricted to pseudobinary alloys, but can be readily extended to ternary systems etc. It is also clear that the total photocurrent (25) can be split up into coherent and incoherent contributions as suggested by Durham [2] for binary alloys. For a more detailed discussion of the averaging procedure used in the case of disordered materials the reader is referred to Durham and Schadler et al. [7].

3. Computational details

All spectra shown in the present paper are based on the KKR-CPA scattering amplitudes for the ground state (Klima et al. [8] and Marksteiner et al. [9]) and ATA-("averaged t-matrix approximation")-like scattering amplitudes for the excited state

$$f_{c,L}^{\mathrm{CPA}}(E) = -\sqrt{E}\, t_{c,L}(E) \tag{27}$$

$$f_l^{\mathrm{ATA}}(E) = \sum_\alpha x_\alpha \sin \delta_l^\alpha(E)\, e^{i\delta_l^\alpha(E)}. \tag{28}$$

In [27] $t_{c,L}(E)$ is the lmth element of the selfconsistent effective t-matrix for the alloyed sublattice (see also Klima et al. [8]) and in (28) the $\delta_l^\alpha(E)$ are the l-like phaseshifts for component α with concentration x_α on this sublattice.

It should be noted that this kind of setup for the excited states was already successfully used by Durham [2] for simple lattice substitutional alloys.

In order to be compatible with the calculation by Johansson et al. [10] for stoichiometric TiN the same computational setup was used: Bulk lattice parameters are assumed even for the surface layer, the surface potential barrier is located such that it touches the muffin-tin spheres in the surface layer. The height of the surface barrier was chosen to be 14.9 eV with respect to the muffin-tin zero and was the same for all vacancy concentrations. To ensure convergence 21 reciprocal lattice vectors are included in the calculation. The electron and hole lifetime broadening parameters are chosen to be −2.0 eV and −0.14 eV for the high energy and low energy states, respectively.

4. Results

In Fig. 1 we compare our theoretical ARUPS for $TiN_{0.83}(100)$ (Fig. 1c) with calculated spectra [10] for stoichiometric TiN(100) (Fig. 1a) and with the experimental spectra [10, 11] for a nominal $TiN_{0.83}(100)$ single crystal (Fig. 1b). The experimental and the two sets of calculated spectra correspond to unpolarised He-I radiation incident along the ⟨011⟩ azimuth at an angle of 45° relative to the surface normal. The escaping photoelectrons are detected at an angle θ_l relative

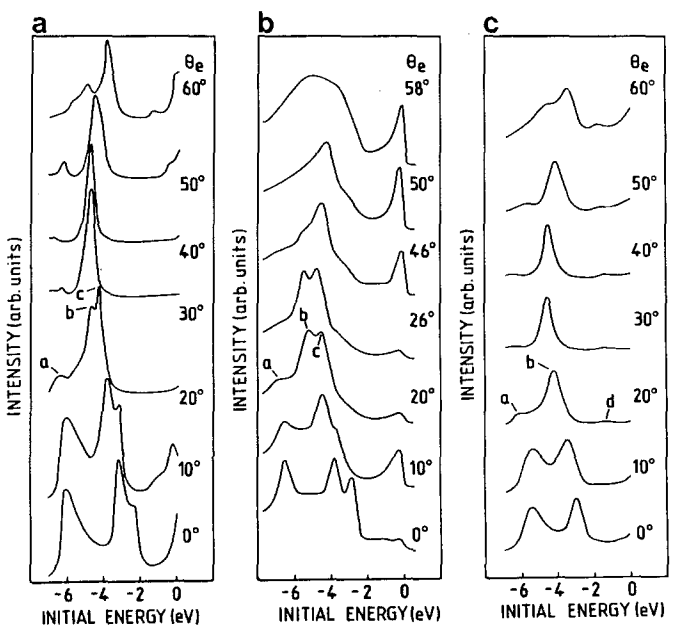

Fig. 1. a Theoretical ARUPS spectra [10] for $TiN_{1.0}(100)$. **b** Experimental ARUPS spectra [10, 11] for $TiN_{0.83}(100)$. **c** Present theoretical results for $TiN_{0.83}(100)$. In Fig. 1a–c unpolarized He-I radiation (21.2 eV) is incident along the ⟨001⟩ azimuth at an angle of 45° relative to the surface normal. The angle of escape of the photoelectrons is denoted by θ_e. In Figs 1a–c peak *a* refers to a Δ_1-like initial state, *b* to a Δ_5-like initial state, *c* to a surface state and *d* to a vacancy induced state

to the surface normal. Using this particular geometry initial states in the ΓXULK plane of the *fcc* Brillouin zone are probed, which means that in the case of normal emission ($\theta_l = 0°$) initial states along the $\Gamma - X$-direction are seen. Using unpolarised radiation implies that initial states of even and odd symmetry with respect to the plane of the incident He-I radiation contribute to the photocurrent (e.g. Δ_1 and Δ_5-like initial states in the case of normal emission).

In all spectra shown in Fig. 1 three peaks are found: peak *a* and *b* are common to all three sets (Fig. 1a–c) of spectra and originate from the Δ_1 and Δ_5-like N-*p* initial states, respectively. Peak *c* is found only in the experimental spectra for $TiN_{0.83}(100)$ (Fig. 1b) and the calculated spectra for stoichiometric TiN(100) (Fig. 1a). This peak was identified as a Tamm surface state [12, 13] separated from the Δ_5-like N-*p* states due to the different potential in the surface layer (as compared to the bulk layers). This feature is reproduced in the calculated spectra only, if proper care is taken of the top layer potential, either by shifting the top layer N-potential by some constant, like in the spectra shown in Fig. 1a or by employing an *ab-initio* surface potential [14].

In the present calculated ARUPS for substoichiometric $TiN_{0.83}(100)$ no such modified top-layer potential was incorporated, since we wanted to emphasize the vacancy-induced changes. Consequently peak *c* is missing in the spectra of Fig. 1c, however, another peak *d* appears for $\theta_l > 10°$. This new peak is due to vacancy induced changes in the electronic structure of $TiN_{0.83}$. Experimentally, this vacancy induced structure is found in angle integrated He-II spectra [15], in XPS spectra [15, 16] and in XES spectra [17] of substoichiometric TiN_X. These findings are summarised in Fig. 2. In fact, the respective calculated spectra [17, 18] which are based on the same KKR-CPA scattering amplitudes used in the present case, show very good agreement with the experimental XPS and XES data.

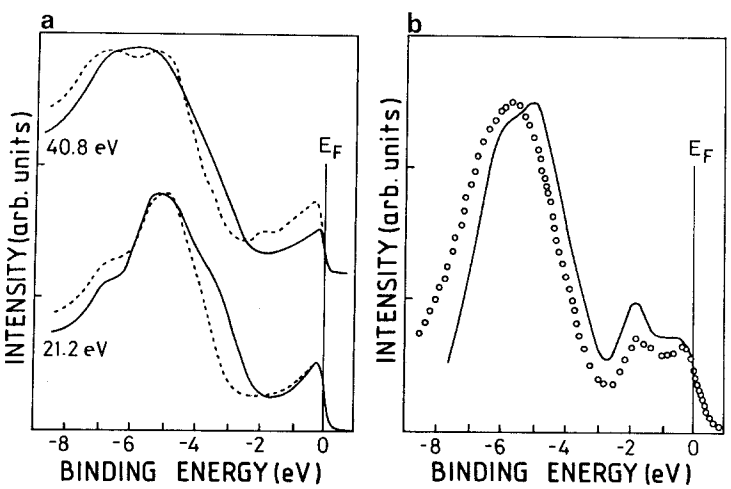

Fig. 2. a Experimental angle integrated valence UPS spectra [15] for $TiN_{1.0}$ (*full line*) and $TiN_{0,80}$ (*dashed line*). **b** Theoretical valence XPS spectrum (*full line*) for $TiN_{0.83}$ [18] and experimental valence spectrum (*circles*) for $TiN_{0.80}$ [15]

This vacancy induced state is not seen in the angle-integrated He-I spectra of $TiN_{0.83}$ [15] shown in Fig. 2a. This is similar to the theoretical findings in the case of normal emission spectra [19] for $TiN_{0.83}(100)$. No vacancy-induced feature is seen for 21 eV photons (cf. Fig. 1c) but the vacancy-state clearly appears for photon-energies higher than 36 eV. This notable difference was explained [19] by the localised nature of the initial vacancy states as opposed to the itinerant character of the N-*p*-like initial states. For He-I energies the big multiple-scattering contributions due to these itinerant states buries the weak atomic-like emission from the localised vacancy-states in the "background". However, if the N-*p* initial states are energetically well separated from the vacancy states, the vacancy states should also show up at this low photon energies. Exactly this situation is encountered in the off-normal spectra for $TiN_{0.83}(100)$ shown in Fig. 1c. A gap in the band structure of stoichiometric TiN opens in the ΓXULK plane as one moves away from the $\Gamma - X$ direction or in other words as soon as one goes to off-normal emission. This gap causes the very low photocurrent around −2 eV seen in the calculated spectra for stoichiometric TiN(100) (Fig. 1a). This gap also favours the "formation" of the (initial) vacancy states as can be seen from the bulk band structure calculations for $TiN_{0.75}$ [20], assuming an ordered defect structure or from Bloch spectral functions in the case of disordered $TiN_{0.75}$ [7]. The vacancy induced peak *d* in the calculated spectra from $TiN_{0.83}(100)$ (Fig. 1c) is not present in the experimental spectra for "$TiN_{0.83}(100)$" (Fig. 1b), and we have to state that the experimental spectra show much better agreement with the calculated spectra for stoichiometric TiN(100) (Fig. 1a). However, in view of the very good agreement with other experimental spectra [17, 18] (cf. Fig. 2b) probing deeper into the bulk, we believe that the present disagreement is not due to our theoretical approach, but is rather caused by a few stoichiometric surface layers of the substoichiometric $TiN_{0.83}(100)$ single crystal employed in the angle-resolved experiments [11]. Indeed, in the most recent experimental studies for $ZrN_{0.93}(100)$ [21] and $TiN_{0.83}(100)$ [22] the theoretically predicted vacancy induced structures [19, 23] were found in normal emission geometry. Since no off-normal spectra were reported in the latter studies, the rather inconsistent experimental results shown in Figs. 1 and 2 have to serve for the purpose of a comparison between the theoretical results and presently available experimental data.

5. Conclusion

The present analysis of experimental and theoretical photoemission spectra for substoichiometric $TiN_{0.83}$ clearly shows that vacancy related features in the electronic structure crucially depend on the actual concentration of vacancies at the surface or in surface near regions. If by sample preparation the bulk vacancy concentration is substantially decreased in the surface, UPS on single crystals maps "stoichiometric spectra", although the sample itself can be highly non-stoichiometric. This kind of experience, however, implies that stoichiometric surfaces can be "grown" systematically on top of non-stoichiometric systems by appropriate tempering methods.

Acknowledgement. This paper was supported by the Austrian Fonds zur Förderung der wissenschaftlichen Forschung (project number P5543). We are most grateful to Dr. P. J. Durham, SERC Laboratory Daresbury, UK, for very helpful discussions.

References

1. Pendry JB (1974) Low energy electron diffraction. Academic Press, New York; JB Pendry (1976) Surf Sci 57:679
2. Durham PJ (1981) J Phys F 11:2475
3. Larsson CG (1985) Surf Sci 152/153:213; Durham PJ, Temmerman WM, Larsson CG, Nilsson PO (1983) Vac 33:771
4. Faulkner JS (1982) Prog Mater Sci 27:1
5. Ham FS, Segall B (1956) Phys Rev 105:108
6 Hopkinson JFL, Pendry JB, Titterington DJ (1980) Comput Phys Comm 19:69
7. Schadler G, Weinberger P, Gonis A, Klima J (1985) J Phys F 15:1675
8. Klima, J, Schadler G, Weinberger P, Neckel A (1985) J Phys F 15:1307
9. Marksteiner P, Weinberger P, Neckel A, Zeller R, Dederichs PH (1986) Phys Rev B33:812
10. Larsson CG, Johansson LI, Callenas A (1984) Solid State Commun 49:727; Johansson LI, Larsson CG, Callenas A (1984) J Phys F 14:1761
11. Johansson LI, Callenas A, Stefan PM, Christensen AN, Schwarz K (1981) Phys Rev B24:1883; Johansson LI, Stefan PM, Shek ML, Christensen AN (1980) Phys Rev B22:1032
12. Johansson LI, Callenas A (1981) Solid State Commun 42:299
13. Inglesfield JE, Callenas A, Johansson LI (1982) Solid State Commun 44:1321
14. Redinger J, Weinberger P, Wimmer E, Neckel A, Freeman A J (1985) Phys Rev B32:6993
15. Hochst H, Bringans RD, Steiner P, Wolf T (1982) Phys Rev B25:7183
16. Porte L, Roux L, Hanus J (1983) Phys Rev B28:3214
17. Beauprez E, Hague CF, Mariot J-M, Teyssandier F, Redinger J, Marksteiner P, Weinberger P (1986) Phys Rev B34:886
18. Redinger J, Marksteiner P, Weinberger P (1986) Z Phys B63:221
19. Redinger J, Weinberger P, Neckel A (1987) Phys Rev B35:5647
20. Herzig P, Redinger J, Eibler R, Neckel A: VIII. International Conference of Solid Compounds of Transition Elements, April 9–13 1985 Vienna/Austria (Extended Abstracts P2 B2)
21. Lindstrom J, Johansson LI, Callenas A, Law DSL, Cristensen AN, Phys Rev B, submitted for publication
22. Lindberg PAP, Johansson LI, Lindstrom JB, Law DSL, Phys Rev B, submitted for publication
23. Redinger J, Weinberger P (1987) Phys Rev B35:5652